Cu(I) chelated poly-alkoxythiophene enhancing photovoltaic device composed of a P3HT/PCBM heterojunction system†

I-Che Wu,[a] Cheng-Hsuan Lai,[a] Dong-Yi Chen,[a] Chun- Wei Shih,[a] Ching-Yen Wei,[b] Bao-Tsan Ko,[bc] Ching Ting[b] and Pi-Tai Chou*[a]

Received 27th March 2008, Accepted 18th July 2008
First published as an Advance Article on the web 22nd August 2008
DOI: 10.1039/b805141k

We report the Cu^+ chelated poly-alkoxythiophene (P3MEET) enhancement of a solar cell device consisting of a P3HT/PCBM heterojunction system. Compared to the reference P3HT/PCBM system, a consistent increase of conversion efficiency of 0.9% *via* an apparent increase of incident-photon-to-current conversion efficiency (IPCE) is achieved upon optimizing the ratio of P3MEET-Cu^+ : P3HT : PCBM to 1 : 9 : 6 by weight, in which 7.5 mol% of CuBr is added upon synthesizing P3MEET-Cu^+. The results, in combination with relevant data gathered from atomic force microscopy, cyclic voltammetry, and electrochemical impedance spectra, lead us to conclude that the match in redox potential and increase of ordering of the film upon doping P3MEET-Cu^+ play two key roles in enhancing the performance.

Introduction

Polymer solar cells, a relatively novel technology, have been attracting intensive research especially due to the recent energy crisis. When compared with the efficiency of inorganic solar cells of as high as 20% and the development of inorganic thin-layer and multi-junction devices, which will likely lead to even better performance,[1–3] the efficiency of ~5% for the best polymer solar cells made so far seems relatively low. However, polymer solar cells have several advantages: they are lightweight, disposable, facile to fabricate, flexible and inert to environmental impact, *etc*. As for the future prospects, they can be a low-cost alternative electricity source with variable shapes and sizes produced by appropriate technology.

Polymer solar cells are commonly realized as "bulk heterojunctions", in which the active layer is mainly composed of an organic polymer as the electron donor and an organic molecule as the electron acceptor.[4] Among various organic polymers suited for solar cells, polythiophene (PT) is environmentally stable in both neutral and doped forms and has conductivity as high as 500 S cm^{-1}.[5] The 3-substituted thiophenes performed especially well; in particular, the highly processable poly(3-alkylthiophene)s (P3ATs) and relevant substituted thiophenes have been the subject of intense research for the past decade.[6–13] Although the attachment of pendant groups does not lead directly to low band gap materials, the presence of electron donating substituents may raise the energy of the highest occupied molecular orbital (HOMO) and turns out to be the most direct and straightforward approach to reduce the band gap of a conjugated backbone. In particular, owing to the mesomeric effect, the narrowing of the energy gap upon adding alkoxy pendants seems to be more promising.[14] Incorporation of alkoxy groups with carbon numbers varying from 1 to 15 on the 3-position of the thiophene ring results in polymers with a low lying transition at 475–530 nm. This is comparable to the absorption maximum of P3ATs. Unfortunately, due to the low molecular weight, the conductivity was generally low. The oxidation potential is also low due to the electron-donating characteristics of the oxygen.[14–16] However, several other alkoxy-substituted analogues of PTs showed characteristic doping effects. For example, McCullough and Williams[17] prepared thin films of head-to-tail poly[3-(2,5,8-trioxanonyl)thiophene] by slow evaporation of $CHCl_3$ solution, followed by oxidization *via* exposure to I_2 vapor. As a result, conductivities up to 5500 S cm^{-1} were measured. This has stimulated practical approaches regarding the synthesis of various novel functional conducting polymers.[18,19]

In yet another approach, polyalkoxythiophenes may also act as good metal sensors. Different metal ions can cause different conformation changes of polyalkoxythiophenes, among which some conformations are found to be more ordered and have a lower band gap. Apart from the metal sensor, polyalkoxythiophene can easily introduce metal ions into the polymer, resulting in drastic changes to its physical, optical and electrochemical properties.[20–22]

In light of the above advantages, we proposed that doping metal ion encapsulated polyalkoxythiophene into the active layer of the prototypical P3HT/PCBM system may improve the morphology and electron/hole mobility as well as the electrochemical properties of the corresponding solar cells, such that a net positive gain is anticipated. Through intensive investigations, we report herein the Cu^+ chelated poly-alkoxythiophene

[a]*Department of Chemistry, National Taiwan University, Taipei, 106, Taiwan. E-mail: chop@ntu.edu.tw; Fax: +886-2-23695208; Tel: +886-2-23630231 ext. 3988*
[b]*Materials and Chemical Laboratories, Industrial Technology Research Institute, Hsinchu, 310, Taiwan*
[c]*Department of Chemistry, Chung Yuan Christian University, Chung-Li 320, Taiwan*

† Electronic supplementary information (ESI) available: Further experimental details; TOF-SIMS, EDS, XANES and absorption spectra; Bode phase plot; *J–V* curves; diagram of device structure. See DOI: 10.1039/b805141k

(P3MEET) enhancement of a solar cell device consisting of a P3HT/PCBM heterojunction system. Compared to the reference P3HT/PCBM system, a consistent increase of conversion efficiency of 0.9% *via* an apparent increase of incident-photon-to-current conversion efficiency (IPCE) is achieved upon optimizing the ratio of P3MEET-Cu^+ : P3HT : PCBM to 1 : 9 : 6 by weight. The results, in combination with relevant data gathered from atomic force microscopy (AFM), time-of-flight (TOF), cyclic voltammetry (CV), and electrochemical impedance spectra, lead us to propose that the match in redox potential and increase of ordering of the film upon doping P3MEET-Cu^+ play dual key roles in enhancing the performance. Details of results and discussion are described in the following sections.

Experimental

Materials

All reactions were conducted under pre-purified nitrogen or argon, using either flame-dried or oven-dried glassware. All glassware was assembled while hot and cooled under nitrogen or argon. Ice/water and dry ice/acetone were used for 0 and −78 °C baths, respectively. Commercial chemicals such as [1,3-bis(diphenylphosphino)propane]dichloronickel(II)) ($Ni(dppp)Cl_2$), sodium hydride (NaH), Grignard reagent, and copper(I) bromide (CuBr) (98%, Acros) were used without further purification. *N*-Bromosuccinimide (NBS) was recrystallized from acetic acid and was dried under vacuum for over 12 h. Prior to use, tetrahydrofuran (THF) was dried and distilled from sodium benzophenone ketyl. All alcohols were dried. Chloroform was dried over CaH_2 for 12 h and distilled prior to use.

Measurement and device preparation

H NMR and ^{13}C NMR spectra were recorded on Varian Unity 400 or Bruker Avance 400 spectrometers at 400 MHz and 100 MHz, respectively. Chemical shifts (δ) are quoted in parts per million (ppm) and coupling constants (J) are recorded in Hertz (Hz). All NMR spectra were recorded in deuterated chloroform ($CDCl_3$) and solvent contained 0.003% TMS as an internal reference. The molecular weight and molecular weight distribution of the synthesized polymers were measured with a Waters GPC (Breeze system) using THF as an eluent at 35 °C. The apparatus was equipped with two Waters Styragel columns (HR3 and HR4E), a refractive index detector (Waters 2414) and a dual-wavelength absorbance detector (Waters 2487). Polystyrene standards (Waters) were used for calibration.

The analysis of Cu concentration was conducted using ICP-MS (Agilent 7500ce) at the Center of Instrumentation Center, National Tsing Hua University. The samples were prepared by microwave digestion with a CEM MARS 5 microwave digestion system.

The X-ray absorption experiments (XANES) were carried out at the National Synchrotron Radiation Research Center (NSRRC), Hsinchu, Taiwan. All Cu K-edge spectra were recorded at room temperature at the wiggler beamline 17C with a double Si(111)-crystal monochromator. The energy resolution $\triangle E/E$ is 2×10^{-4}. High harmonics were removed by using Rh-coated mirrors.

Steady-state absorption was recorded by a Jasco V-570 UV-vis spectrophotometer. All electrochemical experiments were performed with a potentiostat/galvanostat (PGSTAT 12, AUTOLAB). Cyclic voltammetry scanned at a rate of 100 mV s^{-1} in deoxygenated acetonitrile solutions containing 0.1M tetrabutylammonium perchlorate (TBAP). All measurements were carried out at room temperature with a conventional three-electrode configuration consisting of a platinum working electrode, a platinum wire auxiliary electrode, and a nonaqueous $Ag/AgNO_3$ reference electrode. The potentials were referred against the ferrocene internal standard. The AC impedance measurements of all devices were measured under constant light illumination of 100 mW cm^{-2}.

The organic photovoltaic devices of polythiophene/fullerene-based bulk heterojunction solar cell consist of an anode, an active layer, and a cathode, as shown in Fig. S8 of the ESI.† The anode was composed of a modified poly(3,4-ethylenedioxythiophene) : poly(styrene sulfonate) (PEDOT:PSS) layer (*ca.* 30 nm) by spin coating on indium-tin oxide (*ca.* 150nm) onto a glass substrate (area = 0.04 cm^2). The glass substrate coated with ITO (Delta Technologies, $R_s = 10\ \Omega\ cm^{-2}$) was specially cleaned in an ultrasonic bath with detergent, deionized (DI) water, acetone, and isopropyl alcohol. In our experiments, the active-layered blends were configured as Cu(I)-P3MEET/P3HT/PCBM with an optimized weight ratio of 1 : 9 : 6 (P3HT = 13.5 mg) and were prepared by magnetically stirring for 48 h and then filtered using 0.2 μm syringe filters. The active layers of polymer photovoltaic devices were fabricated by spin-coating (1500 rpm) the blends on ITO substrate coated with PEDOT:PSS. The cathode consisted of LiF (*ca.* 0.5 nm)/Al (*ca.* 100 nm) coated by a thermo-evaporated method.

Light-to-electricity conversion efficiency values were measured using a standard AM1.5 solar simulator Oriel 66 924 Arc lamp source with a 6266 450 W Xe lamp, coupled with an Oriel 81088 Air Mass 1.5 Global Filter and a digital source meter purchased from the Keithley company. The incident light intensity was calibrated by using a standard solar cell composed of a crystalline silicon solar cell and an IR cutoff filter (Schott, KG-5), giving a photoresponse range similar to that of an amorphous silicon solar cell.

The sample for TOF measurement was prepared by dip-coating, and dried under vacuum, followed by the evaporation of an Al electrode under vacuum (10^{-5} Torr). A TH (third-harmonic) of a Nd:YAG laser was used to generate the excitation pulse (λ = 355 nm). The transient photocurrent was monitored using an Agilent infiniium Oscilloscope (500 MHz, 1GSa/s).

Results and discussion

Synthesis strategy

***rr*-Poly(3-[2-(2-methoxyethoxy)ethoxy]thiophene) containing CuBr (CuBr-P3MEET).** Scheme 1 depicts the synthetic pathway to CuBr-P3MEET. Details of synthetic procedures are described in the ESI.† First, substitution of 3-bromothiophene with 2-(2-methoxyethoxy)ethanol was carried out to yield alkoxythiophene **3** with a yield of approximately 90%. 2,5-Dibromo-[2-(2-methoxyethoxy)ethoxy]thiophene, *i.e.*, monomer **2**, was then synthesized *via* bromination by using NBS in THF–AcOH mixed

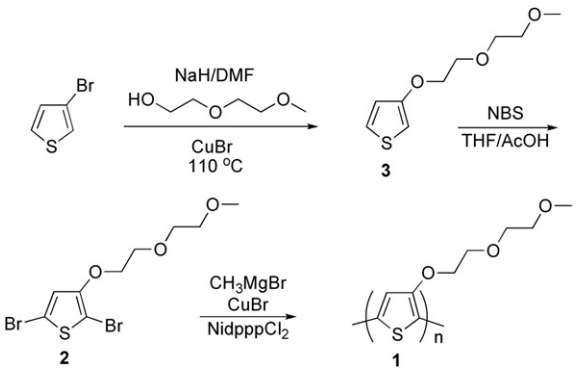

Scheme 1 Synthetic pathways of *rr*-poly(3-[2-(2-methoxyethoxy)ethoxy]-thiophene) (**1**, P3MEET).

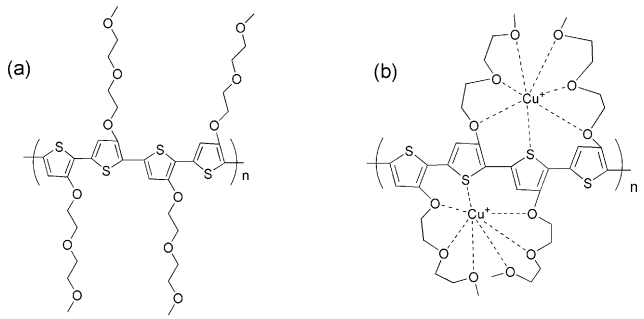

Scheme 2 A qualitative 2D illustration of the polymer backbone conformation (a) without and (b) with copper(I) ion complexation.

solvent at room temperature. In this approach, instead of direct polymerization using **2**, a catalytic amount of CuBr was added to react with Grignard reagent during the polymerization process. As a result, the quantity of CuBr directly reflected the properties of the resulting polymer in *e.g.* optics, electrochemistry, *etc.* (*vide infra*). Additionally, we also noticed that adding a catalytic amount of CuBr increased the polymerization rate. This may be rationalized by the fact that CuBr readily reacts with Grignard reagent (RMgX) *via* transmetallation, forming RMgCuBrX, a softer reagent that has been commonly applied in 1,4-addition to reduce the activation energy and hence to improve the synthesis efficiency.[23]

After the injection, the mixture was stirred for one hour in ambient temperature before Ni(dppp)Cl_2 (0.5 mol%) was poured into the reaction mixture. The head-to-tail-coupled regioregular dark blue polymers **1** (P3MEET) containing various amounts of CuBr were then obtained in very good yield of ~80%. Further purification by Soxhlet extraction with MeOH, n-hexane and CH_2Cl_2 was then carried out. The extracted polymer was collected with $CHCl_3$ and dried under vacuum, yielding a dark brown, metal-like cluster polymer with *e.g.* M_n of 8910 and a PDI of 1.39 using 7.5 mol% of CuBr. Cu ion was found by the characteristic peak on EDS and TOF-secondary ion mass spectroscopy (SIMS, see ESI†). A quantitative analysis of Cu^+ content was performed using the ICP-MS technique. The Cu^+ content in the as-prepared P3MEET-Cu^+ was found to be 9.48×10^3 ppm. The mol% of Cu^+ was then calculated to be ~3%. Further identification of Cu(I) ion was given by the X-ray absorption spectra, in which a peak appearing at 8982 eV is unambiguously assigned to the Cu(I) 1s → 4p transition (see ESI†). In a qualitative manner, graphic depicting the P3MEET backbone conformations without and with Cu(I) encapsulation are shown in Scheme 2a and b, respectively, for the convenience of further discussion. The prepared Cu(I)/P3MEET were readily soluble in many common organic solvents such as CH_2Cl_2 and $CHCl_3$, *etc.*, and possessed excellent film-forming abilities.

Physical and photophysical properties

Fig. 1 shows the absorption spectra (in CH_2Cl_2) of P3MEET and P3MEET reacted with various concentrations of CuBr. The absorption spectrum of CuBr-free P3MEET is characterized by a lowest-lying absorption band maximized at 610 nm (2.03eV),

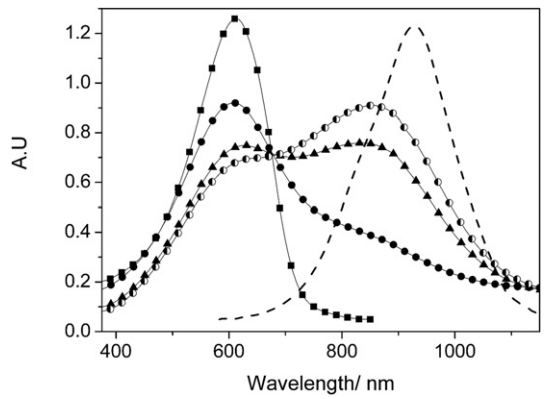

Fig. 1 Absorption spectra of P3MEET reacted with different concentrations of CuBr in CH_2Cl_2: a) 0 mol% (-■-■-); b) 1.5 mol% (-●-●-); c) 5 mol% (-▲-▲-); d) 10 mol% (-◐-◐-). Dashed line shows the emission spectrum of P3MEET in CH_2Cl_2 (excitation wavelength: 580 nm).

which is reasonably ascribed to the thiophene backbone $\pi \rightarrow \pi^*$ transition. Upon electronic excitation (*e.g.* $\lambda_{ex} = 580$ nm), a near infrared emission maximized at ~930 nm was resolved (see Fig. 1), the spectral feature of which revealed a mirror image with respect to the corresponding absorption profile, confirming the 610 nm absorption band to be the lowest-lying transition (in singlet manifold) for P3MEET.

Upon increasing the CuBr concentration, a new absorption band gradually appeared at ~850 nm, accompanied by a decrease of the 610 nm absorption band. This phenomenon is reminiscent of the ionochromic effect reported in previous literature. Swager and Marsella[20] reported that polythiophenes functionalized with alkyl ether chains or crown ethers exhibited significant ionochromic response toward alkaline cations. Such responsiveness is mainly caused by the conformational changes of polythiophenes. The effect of metal ions on polythiophenes anchored with chelate binding units, such as bipyridines and ether chains, was also reported.[21,23] Accordingly, there plausibly exists a non-covalent, electrostatic (ion–dipole) interaction between the oxygen of the ether side chains in P3MEET and Cu(I) (see Scheme 2b), the result of which restricts the free rotation around the thiophene–thiophene bond and consequently drives the backbone of P3MEET from a non-planar conformation to a more planar one. In conjugated polymers, there is a strong correlation of the electronic structure *versus* the

backbone conformation. The increase of the 850 nm band implies that Cu(I) induces the part of the disordered form of P3MEET and transforms it to the more ordered, planar forms. Upon exciting the Cu(I) encapsulated P3MEET around the absorption peak wavelength (*i.e.* 800–850 nm), the emission was too weak to be resolved in the region of >850 nm.

Based on similar synthesis protocols we have also made attempts to replace CuBr with other metal ion salts, such as $CuBr_2$, $ZnCl_2$, $Cd(II)Cl_2$ or $Pt(II)Cl_2$ and encapsulate the corresponding metal ion into P3MEET. Such an encapsulation process was then monitored for changes of optical properties in P3MEET (see ESI†). With the same added concentrations of metal ions, as monitored by the absorption spectral changes, the effect is much less than that of adding Cu(I). One plausible explanation may lie in the fact that P3MEET has the best response to Cu(I) (~0.6–0.7 Å)[24] due to its oxygen cavity size being similar to the radius of copper(I).

In yet another approach, we have attempted to add a similar amount of CuBr to the as-prepared P3MEET. As shown by a very small increase of the 850 nm peak (see ESI† Fig. S4), the addition of CuBr to the already prepared P3MEET only causes slight changes of the backbone conformation. The difference is believed to be due to the different encapsulation sites and/or binding affinity of Cu^+ in P3MEET between these two methodologies, although the actual mechanism is still pending resolution. The facile CuBr incorporation may be rationalized, in part, by the prompt reaction between CuBr and the Grignard reagent (RMgX) for polymerization, forming RMgCuBrX, a soft addition reagent that facilitates the polymerization to increase the synthesis efficiency (*vide supra*). Moreover, the solubility and film forming properties of other metal ion encapsulated P3MEET samples were found to be worse than those of Cu(I)/P3MEET. Thus, the device properties using other metal ion encapsulated P3MEET were not further pursued.

We then measured the oxidation potentials of P3MEET and P3MEET-Cu(I) by cyclic voltammetry (CV) with ferrocene as the reference. As listed in Table 1, P3MEET possessing an alkoxyl substituent of an electron-donating nature at the C(3) position has a HOMO value of −5.21 eV, which is slightly higher in energy than the HOMO value of P3HT (−5.23 eV). After the reaction with CuBr, as revealed in Table 1, the oxidation potential of P3MEET-Cu(I) shifted anodically to −5.33 eV. This result may be rationalized by the fact that complexation of metal cation (Cu(I)) in the cavity, formed by the ether oxygen sites, should decrease the electron donating strength of the ether group due to the electrostatic interaction between Cu(I) and ether oxygen[25] As a result, oxidation of P3MEET becomes more difficult due to the electron-withdrawing effect of the positively charged metal cations in the vicinity of the conjugate polymeric backbone, resulting in an increase of the oxidation potential. This turns out to be one of the crucial factors in the improvement of device performance described below.

Table 1 Electrochemical data of P3HT, P3MEET and P3MEET-Cu^+ in CH_3CN

Polymer	E_{ox}/V[a]	HOMO/eV[b]	LUMO/eV[b]	Energy gap/eV[c]
P3HT	0.85	−5.23	−3.53	1.7
P3MEET	0.83	−5.21	−3.56	1.65
P3MEET-CuBr	0.95	−5.33	−4.13	1.2

[a] Values obtained with 1.0×10^{-3} M solutions of all polymers using 0.10 M tetrabutylammonium perchlorate (TBAP) as the supporting electrolyte. The redox potentials were calibrated using Fc/Fc^+.[b] The energy levels of the HOMO and LUMO were calculated using: HOMO [eV] = $E_{ox} - E_{Fc/Fc+} + 4.8$.[c] Energy gap calculated from the onset of the S_1 band of each polymer.

Device properties

To evaluate the solar cell performance, we first varied the ratio of P3MEET-Cu^+ : P3HT : PCBM by weight, in which the amount of CuBr (% by weight) added to the P3MEET polymerization was kept constant for each batch. As listed in Table 2, the devices **B**, **N1**, **N2**, **N3**, **N4**, and **N5** were prepared with the same P3HT/PCBM weight ratio of 9 : 6, a typical format for making the corresponding P3HT/PCBM solar cell, while the weight ratio of P3MEET-Cu(I) was varied by 0, 0.5, 1, 2, 3, and 4. In each case, Cu(I) was kept at 7.5 mol% during the synthesis of P3MEET-Cu^+. Details of the device making are provided in the Experimental section. The results listed in Table 2 indicate that the device performance, in terms of power conversion efficiency (η (%)), increases upon increasing the weight ratio of P3MEET-Cu^+ from 0 (**B**) to 0.5 (**N1**) and reaches a peak (η (%) = 3.95) at a weight ratio of P3MEET-Cu^+ of 1.0 (**N2**), and then it gradually decreases to η (%) = 1.90 at a weight ratio of P3MEET-Cu^+ of 4.0 (**N5**). More importantly, the trend is reproducible in that devices **N1**, **N2** and **N3** are consistently higher in η (%) than is **B** (no presence of P3MEET-Cu^+). We also realize that there should be a subtle increase of maximum η (%) in the vicinity of the weight ratio of P3MEET-Cu^+ of 1.0. However, our main focus in this study is to probe the function of P3MEET-Cu^+ incorporated in the device. To simplify the discussion, fine-tuning the ratio for P3MEET-Cu^+ *versus* P3HT/PCBM was not further pursued

For control experiments, we also performed photovoltaic measurements based on P3MEET/PCBM and P3MEET-Cu^+/PCBM configurations. The ratio for either P3MEET-Cu^+ : PCBM or P3MEET : PCBM is 9 : 6. As shown in Fig. S7 of the ESI,† much inferior photovoltaic performance is observed for both P3MEET/PCBM and P3MEET-Cu^+/PCBM configurations. The η value was measured to be 2.7×10^{-3}% and 6.5×10^{-4}% for P3MEET/PCBM and P3MEET-Cu^+/PCBM systems,

Table 2 Characters of the all devices with varied conditions

	Devices[a]									
	B	**N1**	**N2**	**N3**	**N4**	**N5**	**D0**	**D5**	**D7.5**	**D10**
J_{sc}/mA cm^{-2}	10.01	10.85	11.98	12.07	9.77	8.15	8.36	11.52	12.32	11.12
V_{oc}/V	0.6	0.6	0.61	0.58	0.58	0.52	0.34	0.54	0.6	0.59
η (%)	3.12	3.27	3.95	3.33	2.72	1.90	1.07	3.54	4.07	3.37
FF	0.52	0.50	0.55	0.48	0.48	0.45	0.39	0.56	0.55	0.51

[a] The devices **B**, **N1**, **N2**, **N3**, **N4**, and **N5** have the same P3HT/PCBM weight ratio (9 : 6), while varying the weight ratio of Cu-P3MEET by 0 (**B**), 0.5 (**N1**), 1 (**N2**), 2 (**N3**), 3 (**N4**), and 4 (**N5**); for **D0**, **D5**, **D7.5**, and **D10** devices, the ratio of P3MEET-Cu^+ : P3HT : PCBM in the active area has been optimized to 1 : 9 : 6 by weight with varying molar ratio of CuBr : **D0** (0 mol%), **D5** (5 mol%), **D7.5** (7.5 mol%) and **D10** (10 mol%).

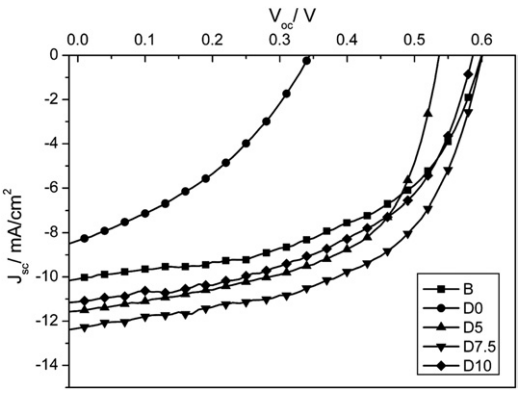

Fig. 2 *I–V* characteristics of various devices made by varying the molar ratio of CuBr: **D0** (0 mol%), **D5** (5 mol%), **D7.5** (7.5 mol%) and **D10** (10 mol%). Note that in **D0**, **D5**, **D7.5**, and **D10** devices, the ratio of P3MEET-Cu^+ : P3HT : PCBM in the active area was optimized to 1 : 9 : 6 by weight, and **B** device contains no Cu-P3MEET.

respectively. As elaborated in the later section, poor film morphology should account for the inferior performance.

We then made devices at a weight ratio of 1 : 9 : 6 for Cu(I)/P3MEET : P3HT : PCBM for the active-layered components, but varied the molar ratio of CuBr added to the reaction, forming Cu(I)/P3MEET, and specified the corresponding devices as **D0**, **D5**, **D7.**5, and **D10**, which had 0 mol%, 5 mol%, 7.5 mol%, and 10 mol% of CuBr, respectively. Again, note the basic device **B** was configured by the weight ratio (P3HT : PCBM) of 9 : 6 and served as a reference.

Typical resulting *I–V* curves of the solar-cell devices **B**, **D0**, **D5**, **D7.5**, and **D10** are depicted in Fig. 2, while pertinent data are listed in Table 2. The power conversion efficiencies (η (%)) for **B**, **D0**, **D5**, **D7.5**, and **D10** were 3.12%, 1.07%, 3.54%, 4.07% and 3.37%, with current densities (J_{sc}) of 10.01, 8.36, 11.52, 12.32 and 11.12 mA cm^{-2}, respectively. The open-circuit voltages (V_{oc}) were measured as 0.6 (**B**), 0.34 (**D0**), 0.54 (**D5**), 0.60 (**D7.5**) and 0.59 V (**D10**). Accordingly, the filled factors (FF) for **B**, **D0**, **D5**, **D7.5**, and **D10** were then calculated as 0.52, 0.39, 0.56, 0.55 and 0.51, respectively. Pertinent data suitable for discussion are also summarized in Fig. 3. Obviously, there is a large difference in the open-circuit voltage between device **B** and device **D0**, which drops from 0.60 V to 0.34 V (see Fig. 2 and 3). In fact, V_{oc} for **D0** is also significantly smaller than that of other devices by more than 200 mV. The results can be rationalized by the energy level diagram estimated *via* the combination of CV and UV-near IR absorption data listed in Table 1. As measured by CV (*vide supra*), the HOMO energy level of CuBr free P3MEET is higher than the HOMO energy level of P3HT. Upon excitation, the higher P3MEET HOMO energy level (*c.f.* HOMO of P3HT) leads to the transport of hole carriers endergonically, causing an accumulation of hole carriers at the HOMO of P3MEET. Therefore, electron carriers in the active layer of the device **D0** facilely recombine with the hole carriers accumulated at P3MEET. For this case, it is reasonable to predict a decrease of the parallel resistance, R_p, of the photovoltaic device **D0** when the electron–hole recombination occurs in the active layer. The relationship between V_{oc} and R_p can be expressed as

$$V_{oc} = \frac{nk_B T}{q} \ln\left(\frac{J_{ph}(V_{oc})}{J_S} + 1 - \frac{V_{oc}}{J_S R_p}\right) \quad (1)$$

where J_{ph} is the photocurrent source, J_S is the reverse saturation current, R_p is parallel resistance, and k_B is the Boltzmann constant.[26] According to eqn (1), the reduction of R_p, in theory, causes a significant decrease of the open-circuit voltage, as observed in device **D0**.

By comparing the current density, J_{sc}, of device **B** with respect to those of devices **D5**, **D7.5**, and **D10**, we found that the J_{sc} of the photovoltaic devices increased with increasing concentrations of Cu(I) added in the polymerization reaction. This was especially obvious in devices **D7.5** and **B**, as the difference in J_{sc} was as large as 2.3 mA cm^{-2}. One plausible reason why J_{sc} is enhanced by the addition of Cu(I) through the alkoxy-substituted side chain lies in the fact that the HOMO energy level of Cu(I)/P3MEET is lowered by coordination with Cu(I) (*vide supra*). Accordingly, a cascade-energy-level framework is established among P3HT/P3MEET-Cu^+/PCBM, as depicted in Scheme 3, resulting in facilitation of electron (hole) transporting efficiency. For further verification, the electron mobility for P3MEET-Cu^+ modified photovoltaic systems was measured with the TOF technique. As depicted in Fig. 4, the results show a trend that the electron mobility of device **D7.5** is higher than that of device **B**. This result clearly indicates that the charge transport properties can be increased by blending decent P3MEET-Cu^+ with P3HT and PCBM in bulk heterojunction solar cell.

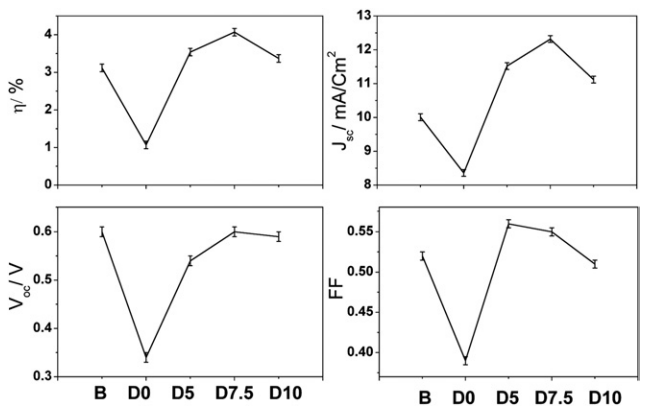

Fig. 3 The electronic properties of the devices **B**, **D0**, **D5**, **D7.5**, and **D10**.

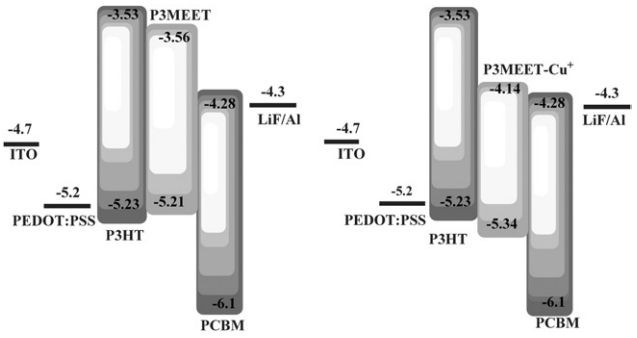

Scheme 3 Energy level diagrams of (a) device **D0** and (b) device **D7.5**. Note the LUMO energy levels for P3MEET and P3MEET-Cu^+ are deduced from the addition of the lowest absorption maximum (in terms of eV) to the corresponding HOMO level.

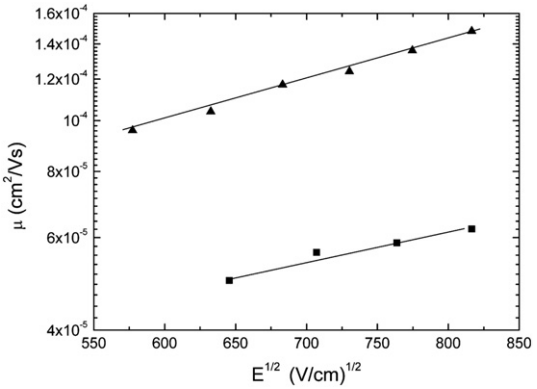

Fig. 4 The comparison of electron (μ_e) mobilities of devices **B** (-■-) and **D7.5** (-▲-) obtained from TOF measurement.

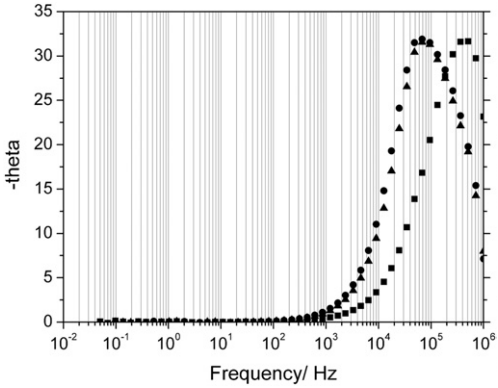

Fig. 6 Bode phase plot of device **B** (▲), device **D0** (■) and device **D7.5** (●) at OCV (−0.6 V), 1 sun.

In order to gain more understanding into the effect of the presence of CuBr on the device performance, prototypical action spectra of incident-photon-to-current conversion efficiency (IPCE) were obtained from polymer photovoltaic devices **B**, **D0** and **D7.5**. Visible light (400–870 nm) could be converted to current with a maximum of 57% efficiency at 510 nm by solar cell **D7.5**, producing a prominent photocurrent of 12.32 mA. Conversely, for devices **B** and **D0**, the IPCE at the peak are 52% and 45%, respectively. Note, as shown by Fig. 5, the absorption of devices **D5**, **D7.5**, and **D10** around 600–800 nm does not convert to any additional photocurrent because of the very minor amount of Cu(I)/P3MEET added in the device, which causes negligible interference to the entire absorption spectra mainly originating from P3HT.

Again, the degradation of IPCE in device **D0** as compared with device **B** can be rationalized by the higher HOMO of P3MEET in **D0** (*vide supra*). As a result, under standard AM 1.5G irradiation, the hole generated in P3HT not only transfers to PEDOT:PSS but also migrates to the HOMO of P3MEET, such that a portion of the electrons and holes may recombine in the extra P3MEET layer. Consequently, the charge separation efficiency in device **D0** becomes lower than that of device **B**. To verify this viewpoint, Bode phase plots of electrochemical impedance spectra were used to confirm this proposed unfavorable quenching process for **D0**. As shown in Fig. 6, the Bode phase plots of three representative devices **B**, **D0** and **D7.5** indicate that the characteristic frequency of device **D7.5** ($\sim 6.2 \times 10^4$ Hz) is lower than those of device **D10** (6.5×10^4 Hz, see ESI†) and **B** ($\sim 6.9 \times 10^4$ Hz). More importantly, compared with those of devices **B** and **D7.5**, the characteristic frequency of device **D0** shifts to a significantly higher frequency of $\sim 5.1 \times 10^5$ Hz, such that the electron lifetime is in the order of **D7.5 > D10 > B ≫ D0**, consistent with the trend in decrease of the power conversion efficiency and J_{sc} (see Table 2). The results provide supplementary support in that the electron lifetime is shortened in the P3MEET layer in device **D0** due to its relatively higher HOMO energy level (*cf.* P3HT) and hence the acceleration of the local electron–hole recombination.[27] On the other hand, the energy level derived from Table 1 and depicted in Scheme 3 clearly shows that the HOMO of Cu(I)/P3MEET in device **D7.5** was relatively lower than those of P3MEET and even P3HT. In device **D7.5**, the lower energy level of the HOMO of Cu(I)/P3MEET predicted the recombination process between PEDOT:PSS and PCBM (LUMO), since the hole carrier generated under irradiation at the P3HT layer can only transfer to the PEDOT:PSS layer. We thus reasonably suggest that Cu(I)/P3MEET in device **D7.5** could act as a hole-transport assisting material, which may serve as one of the factors to increase the J_{sc} and IPCE of device **D7.5**. In theory, this would help to balance the differences between the electron mobility and the hole mobility in the device.

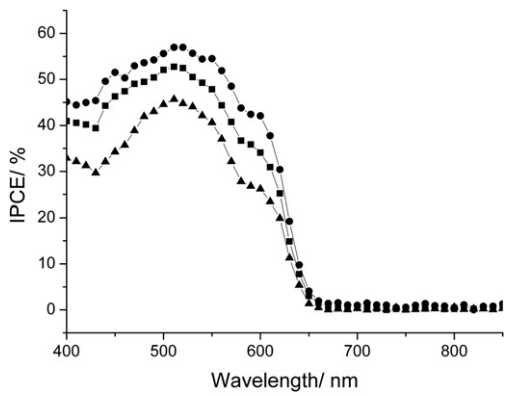

Fig. 5 Incident photon to electron efficiency (IPCE) of device **B** (-■-■-), device **D7.5** (-●-●-) and device **D0** (-▲-▲-) based organic solar cells.

However, despite the cascade-energy level on P3HT/P3MEET-Cu^+/PCBM (see CV results in ESI†), upon further increasing the Cu^+ concentration, device **D10** revealed a lower power conversion efficiency than that of reference **D7.5**, indicating that in addition to the match in redox potential there exist other factors that govern the device performance. As fa plausible alternative, it has been reported that the morphology of the film plays a critical role in achieving higher efficiency in photovoltaic cells.[28] Ordering of morphology in the active layer commonly enhances IPCE and hence the power conversion efficiency. Due to the agreement in the backbone configuration between P3HT and P3MEET-Cu^+, we thus suspect that the improvement in the morphology of the active-layered film may serve as another key factor in enhancing solar cell performance. As such, the atomic force microscopy (AFM) images may provide evidence for the differences in

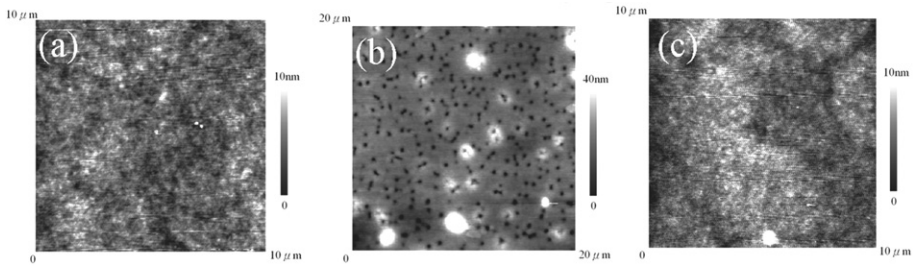

Fig. 7 AFM topography images (10 μm × 10 μm) of (a) device **B**, (b) device **D0**, and (c) device **D7.5** cast from chlorobenzene.

morphology among various devices. Fig. 7 reveals the surface topography of the as-prepared devices **B**, **D0** and **D7.5** acquired by AFM. As shown Fig. 7, it is apparent that the surface morphology of device **D0** (Fig. 7(b)) is significantly worse in view of ordering than those of devices **B** and **D7.5**. The destructive film structure of device **D0** may be caused by the free bending of the alkoxy side chain of P3MEET with the lack of Cu^+ constraint/coordination. Upon Cu^+ coordination to P3MEET, the ordering of morphology shown in **D7.5** (Fig. 7(c)), which is clearly higher than that of the standard P3HT/PCBM device **B** (Fig. 7(a)), is consistent with the observed superior performance in terms of J_{sc}, IPCE and hence η (%) for device **D7.5**.

Conclusions

In summary, regioregular polythiophenes bearing alkoxy chain moieties have been synthesized. The alkoxy-substituted polythiophenes, P3MEET, show high electrochemical stability and conductivity and are capable of chelating metal ions due to the electron-donating properties of the ether oxygen atoms. Among the various metal ions investigated, facile synthesis of Cu^+ chelated P3MEET was reported. Both HOMO and LUMO of P3MEET-Cu^+ reveal decent energy levels, such that the active layer composed of P3HT/P3MEET-Cu^+/PCBM has a cascade-type potential energy diagram (Scheme 3) suitable for promoting P3HT/PCBM solar cell performance. High values for the IPCE of the device composed of P3HT/P3MEET-Cu^+/PCBM as compared to those of P3HT/PCBM have been achieved. Comparing the prototypical P3HT/PCBM system, a consistent increase of conversion efficiency of 0.9% *via* an apparent increase of IPCE is achieved upon optimizing the ratio of P3MEET-Cu^+ : P3HT : PCBM to 1 : 9 : 6 by weight, in which 7.5 mol% of CuBr is added upon synthesizing P3MEET-Cu^+. The results, in combination with relevant data gathered from atomic force microscopy (AFM), cyclic voltammetry (CV), electrochemical impedance spectra and TOF, lead us to conclude that the match in redox potential and increase of ordering of the film upon doping P3MEET-Cu^+ play two key roles in enhancing the performance. At this stage, the actual enhancing mechanism, such as *e.g.* the possibility of P3MEET-Cu^+ acting as a functional compatibilizer, which may be located at the interface of P3HT and PCBM, is pending resolution. Nevertheless, the results achieved in this report should spark the future development of more novel metal ion-chelated polymer for organic solar cell applications.

References

1 F. C. Krebs and H. Spanggaard, *Chem. Mater.*, 2005, **17**, 5235.
2 M. Reyes-Reyes, K. Kim, J. Dewald, R. López-Sandoval, A. Avadhanula, S. Curran and D. L. Carroll, *Org. Lett.*, 2005, **7**, 5749.
3 (*a*) W. Ma, C. Yang, X. Gong, K. Lee and A. J. Heeger, *Adv. Funct. Mater.*, 2005, **15**, 1617; (*b*) M. Reyes-Reyes, D. L. Carroll and K. Kim, *Appl. Phys. Lett.*, 2005, **87**, 083506; (*c*) Y. Yang, V. Shrotriya, J Huang, K Emery, Y. Yao, T. Moriarty and G. Li, *Nat. Mater.*, 2005, **4**, 864.
4 M. C. Scharber, D. Mühlbacher, M. Koppe, P. Denk, C. Waldauf, A. J. Heeger and C. J. Brabec, *Adv. Mater.*, 2006, **18**, 789.
5 M. Sato, S. Tanaka and K. Kaeriyama, *J. Chem. Soc., Chem. Commun.*, 1985, 713.
6 J. H. Borroughes, D. D. C. Bradley, A. R. Brown, R. N. Marks, K. MacKay, R. H. Friend, P. L. Burns and A. B. Holmes, *Nature*, 1990, **347**, 539.
7 Y. Ohmori, M. Uchida, K. Muro and K. Yoshino, *Jpn. J. Appl. Phys.*, 1991, **30**, 1938.
8 T. Kawai, T. Kuwabara, S. Wang and K. Yoshino, *Jpn. J. Appl. Phys.*, 1990, **29**, 602.
9 J. Bobacka, A. Ivaska and M. Grzeszczuk, *Synth. Met.*, 1991, **44**, 9.
10 *Relaxation in Polymers*, ed. T. Kobayashi, World Scientific, Singapore, 1993, pp. 1–79.
11 S. R. Kim, S. A. Choi, J. D. Kim, K. J. Kim, C. Lee and S. B. Rhee, *Synth. Met.*, 1995, **71**, 2027.
12 H. S. O. Chan, S. C. Ng and S. H. Seow, *Synth. Met.*, 1994, **66**, 177.
13 H. S. O. Chan, C. S. Toh and L. M. Gan, *J. Mater. Chem.*, 1995, **5**, 631.
14 S. A. Chen and C. C. Tsai, *Macromolecules*, 1993, **26**, 2234.
15 R. L. Blankespoor and L. L. Miller, *J. Chem. Soc., Chem. Commun.*, 1985, 90.
16 A. C. Chang, R. L. Blankespoor and L. L. Miller, *J. Electroanal. Chem.*, 1987, **236**, 239.
17 R. D. McCullough and S. P. Williams, *J. Am. Chem. Soc.*, 1993, **115**, 11608.
18 M. Feldhues, G. Kampf, H. Litterer, T. Mecklenburg and P. Wegener, *Synth. Met.*, 1989, **28**, C487.
19 M. Leclerc and I. Lévesque, *J. Chem. Soc., Chem. Commun.*, 1995, 2293.
20 T. M. Swager and M. J. Marsella, *J. Am. Chem. Soc.*, 1993, **115**, 12214.
21 P. Bäuerle and S Scheib, *Adv. Mater.*, 1993, **5**, 848.
22 I. Lévesque and M Leclerc, *Chem. Mater.*, 1996, **8**, 2843.
23 R. B. Grossman, *The Art of Writing Reasonable Organic Reaction Mechanisms*, Springer-Verlag, New York, 2nd edn, 2003. p. 297.
24 R. D. Shannon, *Acta Crystallogr., Sect. A*, 1976, **32**, 751.
25 P. Bäuerle and S Scheib, *Acta Polym.*, 1995, **46**, 124.
26 S. R. Forrest, D. P. Rand and B. P. Burk, *Phys. Rev. B*, 2007, **75**, 115327.
27 Q. Wang, J. E. Moser and M. Grätzel, *J. Phys. Chem. B*, 2005, **109**, 14945.
28 J. Peet, J. Y. Kim, N. E. Coates, W. L. Ma, D. Moses, A. J. Heeger and G. C. Bazan, *Nat. Mater.*, 2007, **6**, 497.